

Self-doping effect and possible antiferromagnetism at titanium-layers in the iron-based superconductor $\text{Ba}_2\text{Ti}_2\text{Fe}_2\text{As}_4\text{O}$

Hao Jiang,¹ Yun-Lei Sun,¹ Jianhui Dai,² Guang-Han Cao,^{1,*} and Chao Cao^{2,†}

¹*Department of Physics, State Key Lab of Silicon Materials, and Center for Correlated Matter, Zhejiang University, Hangzhou 310027, China*

²*Condensed Matter Physics Group, Department of Physics, Hangzhou Normal University, Hangzhou 310036, China*

(Dated: July 31, 2012)

The electronic structure of $\text{Ba}_2\text{Ti}_2\text{Fe}_2\text{As}_4\text{O}$, a newly discovered superconductor, is investigated using first-principles calculations based on local density approximations. Multiple Fermi surface sheets originating from Ti-3d and Fe-3d states are present corresponding to the conducting $\text{Ti}_2\text{As}_2\text{O}$ and Fe_2As_2 layers respectively. Compared with BaFe_2As_2 , sizeable changes in the related Fermi surface sheets indicate significant electron transfer (about $0.12e$) from Ti to Fe, which suppresses the stripe-like antiferromagnetism at the Fe sites and simultaneously induces superconductivity. Our calculations also suggest that an additional Néel-type antiferromagnetic instability at the Ti sites is relatively robust against the electron transfer, which accounts for the anomaly at 125 K in the superconducting $\text{Ba}_2\text{Ti}_2\text{Fe}_2\text{As}_4\text{O}$.

PACS numbers: 74.70.Xa; 71.20.Ps; 75.30.Fv; 74.20.Pq

The discovery of high-temperature superconductivity in iron pnictides^{1,2} has triggered stimulated studies in the condensed matter physics field.³ A common feature of these Fe-based superconductors in various families are that they all contain Fe_2X_2 ($X=\text{As}$ or Se) layers in which the Fe moment aligns antiferromagnetically⁴⁻⁷ at the ground state of the parent compounds. Superconductivity emerges if the antiferromagnetism (AFM) is sufficiently suppressed by either chemical doping^{1,8,9} or applying pressures.¹⁰ The electronic structure of the undoped Fe_2X_2 layers is semi-metallic, characterized by two or more hole pockets around the Γ (0, 0) point, and two electron pockets near the X (π , π) point.^{11,12} First-principles studies based on density functional theory (DFT) have been very helpful in obtaining the band structure,¹³ predicting the superconducting pairing symmetry,¹⁴ constructing the theoretical model,¹⁵⁻¹⁷ and reproducing the experimental magnetic ground states.^{14,18,19}

By building new structures containing Fe_2X_2 layers, a new oxypnictide superconductor $\text{Ba}_2\text{Ti}_2\text{Fe}_2\text{As}_4\text{O}$ (Ba22241) was recently discovered.²⁰ The Ba22241 material can be viewed as an intergrowth of BaFe_2As_2 ²¹ and $\text{BaTi}_2\text{As}_2\text{O}$ ²², containing $\text{Ti}_2\text{As}_2\text{O}$ sheets as well as the common Fe_2As_2 layers (see Fig. 1). Although neither BaFe_2As_2 nor $\text{BaTi}_2\text{As}_2\text{O}$ is superconducting, the combined structure—Ba22241—shows superconductivity at 21 K *without doping*. Based on the variation of bond-valence sum (BVS) of Ti, electron transfer from Ti to Fe was proposed to interpret the appearance of superconductivity as a result of self doping.²⁰ Another interesting issue comes from an anomaly at $T^* \sim 125$ K in electrical resistivity and magnetic susceptibility. The origin and the nature of this anomaly remain mysterious because both Fe and Ti sublattices could play a role. It was tentatively ascribed to a possible charge-density wave (CDW) or spin-density wave (SDW) transition in the $\text{Ti}_2\text{As}_2\text{O}$

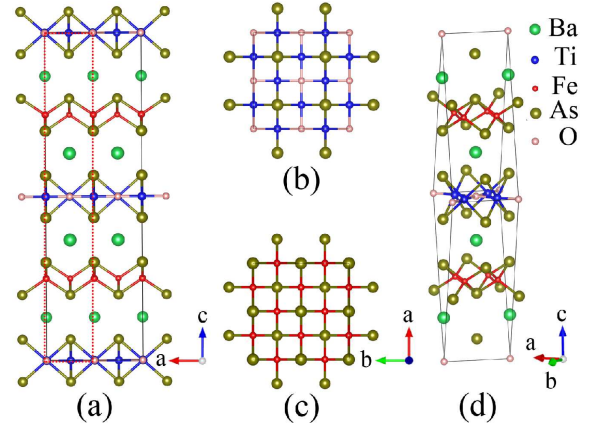


FIG. 1: Crystal structure of $\text{Ba}_2\text{Ti}_2\text{Fe}_2\text{As}_4\text{O}$ superconductor. (a) a [100] side view showing the layered structure containing Ti_2O sheets as well as the common Fe_2As_2 layers. Top views on $\text{Ti}_2\text{As}_2\text{O}$ sheets and Fe_2As_2 are displayed in (b) and (c). A primitive cell is shown in (d).

layers in the original study.²⁰ This proposal was supported by recent Mössbauer experiment which indicates paramagnetic (PM) state, without long-range magnetic ordering below the T^* , for the Fe in Ba22241.²³ So, the Ba22241 material may represent a rare example to show a two-dimensional (2D) CDW/SDW ordering sandwiched by superconducting layers.

To clarify and interpret the above experimental results, in this communication, we present a detailed first-principles study of the Ba22241 electronic structure by DFT calculations, in direct comparison with both BaFe_2As_2 and $\text{BaTi}_2\text{As}_2\text{O}$. It is shown that the density of states (DOS) around Fermi level E_F are dominated by Fe-3d orbitals in the FeAs layers as well as Ti-3d and As-4p orbitals from the $\text{Ti}_2\text{As}_2\text{O}$ layers. The Fermi sur-

face sheets can be regarded as a combination of BaFe_2As_2 and $\text{BaTi}_2\text{As}_2\text{O}$ systems, respectively. Nevertheless, sizeable changes in the corresponding Fermi surface sheets, which means significant electron transfer to the FeAs layers, are induced by the insertion of $\text{Ti}_2\text{As}_2\text{O}$ layers. The charge transfer serves as a self-doping effect, which suppresses the formation of long range magnetic ordering in the FeAs layers and leads to superconductivity without explicit doping. The calculated bare electron susceptibility suggests an AFM instability in the $\text{Ti}_2\text{As}_2\text{O}$ layers, similar to that in $\text{BaTi}_2\text{As}_2\text{O}$. This AFM instability is itinerant in nature, but is weakened compared to that of $\text{BaTi}_2\text{As}_2\text{O}$ due to the self-doping effect, thus it may account for the anomaly at 125 K in Ba22241 .

All reported results are obtained using the DFT as implemented in the Vienna abinitio simulation package (VASP)^{24,25}, where the valence electron-ion interactions are modeled using projected augmented wave (PAW) method^{25,26} and the exchange-correlation effects are approximated with Perdew-Burke-Ernzerhoff flavor of general gradient approximation (PBE).²⁷ To ensure the convergence of the calculations, a 520 eV energy cutoff to the plane wave basis and a $9 \times 9 \times 9$ Γ -centered K-mesh is employed; whereas a $18 \times 18 \times 18$ Γ -centered K-mesh and tetrahedron method are employed to perform the DOS calculations.

Since the Mössbauer experiment results show that long-range magnetic ordering is absent at the FeAs layers, most of our calculations are based on the spin-unpolarized DFT. In fact, due to the systematic overestimation of magnetic energies and moments in spin-polarized DFT calculations of iron-pnictides²⁸, spin-unpolarized DFT calculations in most cases will yield more useful information about the electronic structure of these systems^{28,29}. It has also been shown that the electronic structure of iron-pnictides sensitively depends on the As-height z_{As} , whereas spin-unpolarized DFT calculations of iron-pnictides systematically underestimate z_{As} ²⁸ as well as the crystal c -axis. Similar effect has been observed in our calculations, as both z_{As}^{I} (As^{I} denotes the arsenic atoms close to Fe sheets) and c -axis are substantially smaller (over 9%) than the experimental value after full structural optimization, resulting in a significantly increased As-Fe-As bond angle (120.4° as oppose to the experimental value 112.1°). Thus the experimental structure was adopted to perform calculations unless otherwise specified.

We show the band structure and density of states (DOS) of the nonmagnetic (NM) Ba22241 in Fig. 2. The Fe-3d and Ti-3d orbitals dominate the electronic states near the Fermi level E_F , contributing 38% and 51% of the DOS, respectively. The band dispersion within $E_F \pm 0.5$ eV could be regarded as a simple superposition of BaFe_2As_2 band structure and the $\text{BaTi}_2\text{As}_2\text{O}$ one. Close to E_F , the bands are dominantly Fe- t_{2g} and Ti- e_g orbitals, although the orbital character weight of the latter is significantly reduced due to the hybridization between Ti-3d and As-4p. Interestingly, all the Fe-

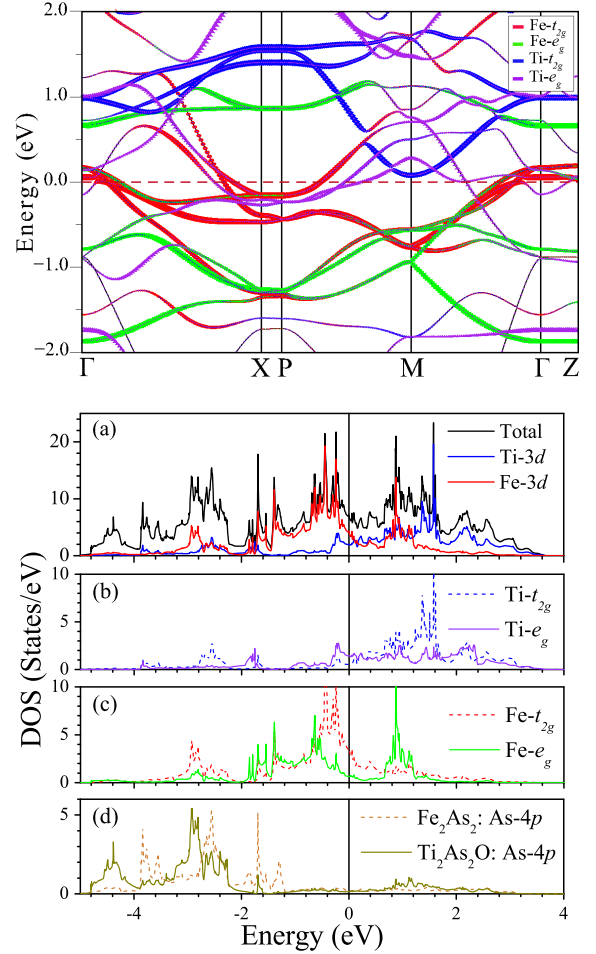


FIG. 2: (Color online) $\text{Ba}_2\text{Ti}_2\text{Fe}_2\text{As}_4\text{O}$ (a) band structures and (b) DOS as well as their projection onto different orbitals. The colors and widths of the lines in (a) represent the orbital character and its weight of the bands, respectively. In both figures, Fermi levels are shifted to zero.

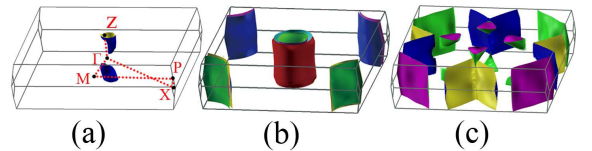


FIG. 3: (Color online) (a) High symmetry points of the body-centered tetragonal primitive cell and the small Fe-related hole pocket around Γ . (b) Fe-related and (c) Ti-related Fermi surface sheets of $\text{Ba}_2\text{Ti}_2\text{Fe}_2\text{As}_4\text{O}$. Notice the shape of Fe-related sheets are very close to those of BaFe_2As_2 .

related bands show little dispersion along $\Gamma - Z$ while most Ti-related bands disperse strongly along that direction, meaning that the FeAs layers are strongly two-dimensional while the $\text{Ti}_2\text{As}_2\text{O}$ -layers are much more isotropic due to more itinerancy for the Ti-3d electrons.

The NM Fermi surfaces were then obtained by fitting the DFT band structure to a tight-binding Hamil-

tonian using the maximally localized Wannier functions (MLWFs)^{30–32}, and interpolating to a dense $100 \times 100 \times 100$ Γ -centered K-grid (Fig. 3). We separate the Ti-related and the Fe-related Fermi surface sheets in Fig. 3. Consistent with the band structure, the Fe-related hole pockets show less dispersion along k_z axis than those of BaFe_2As_2 compound, suggesting an enhanced quasi-2D feature of the FeAs layer. To analysis the charge transfer between FeAs layers and $\text{Ti}_2\text{As}_2\text{O}$ layers, we integrated the volume enclosed by the Fe-related hole-sheets around Γ . Parent BaFe_2As_2 has three hole sheets around Γ , which is integrated to be $0.335|e|$. For Ba22241 , there are also three hole sheets, but the enclosed volume is reduced to $0.215|e|$. Thus, ~ 0.12 electron per unit cell is transferred to the FeAs layer from the $\text{Ti}_2\text{As}_2\text{O}$ layer. This result is qualitatively consistent with both the projected-DOS analysis and an extra Bader charge analysis, which shows charge transfer by ~ 0.05 per unit cell to the FeAs layer. We notice that the quantity of transferred charge is also in good agreement with the BVS analysis.²⁰ Previous studies³ have established that doping will suppress the formation of long-range stripe-like (SL-AFM^{Fe}) order and thus induce the superconductivity. Therefore, we conclude that superconductivity in the undoped Ba22241 is induced by self doping due to the electron transfer from the intercalated $\text{Ti}_2\text{As}_2\text{O}$ layer. It is noted that similar self-doping induced superconductivity was evidenced in $\text{Sr}_2\text{VFeAsO}_3$ superconductor.³³

It is expected that the long range SL-AFM^{Fe} order is suppressed due to the self-doping effect, as also evidenced by the Mössbauer experiment²³. However, this does not imply the absence of magnetic order in the $\text{Ti}_2\text{As}_2\text{O}$ -layers. Itinerant magnetic instability may develop due to the metallic band structure of that layer. Therefore, we calculate the bare irreducible susceptibility using the maximally localized Wannier functions (MLWFs)^{30,31} according to

$$\chi_0(\mathbf{q}) = \sum_{nm\mathbf{k}} \frac{f(\epsilon_{n\mathbf{k}}) - f(\epsilon_{m\mathbf{k}+\mathbf{q}})}{\epsilon_{m\mathbf{k}+\mathbf{q}} - \epsilon_{n\mathbf{k}}}$$

for Ba22241 , $\text{BaTi}_2\text{As}_2\text{O}$, and BaFe_2As_2 compounds, as shown in Fig. 4. It should be noted that the plots for Ba22241 and BaFe_2As_2 are generated using primitive cells, and thus the corresponding Brillouin zone (BZ) needs to be folded to compare with conventional notations and with the $\text{BaTi}_2\text{As}_2\text{O}$ plot. Originally, the formation of SL-AFM^{Fe} order in BaFe_2As_2 is signaled by a large peak at X (π, π) in the folded tetragonal BZ³⁴. For Ba22241 , the (π, π) peak is appreciably broadened, with a cusp forming at its center. It suggests that the original SL-AFM^{Fe} order is becoming unstable in Ba22241 , consistent with the self-doping scenario. In addition to this feature, another strong sharp peak at M ($\pi, 0$) (notation in the conventional tetragonal BZ) can be identified in Ba22241 . This signals certain electronic instabilities. Using the rigid band model, we have also obtained χ_0 of Ba22241 at different doping concentrations ($x=0.0, 0.1$ and 0.2) [Fig. 4(a)]. The (π, π) peak corresponding to

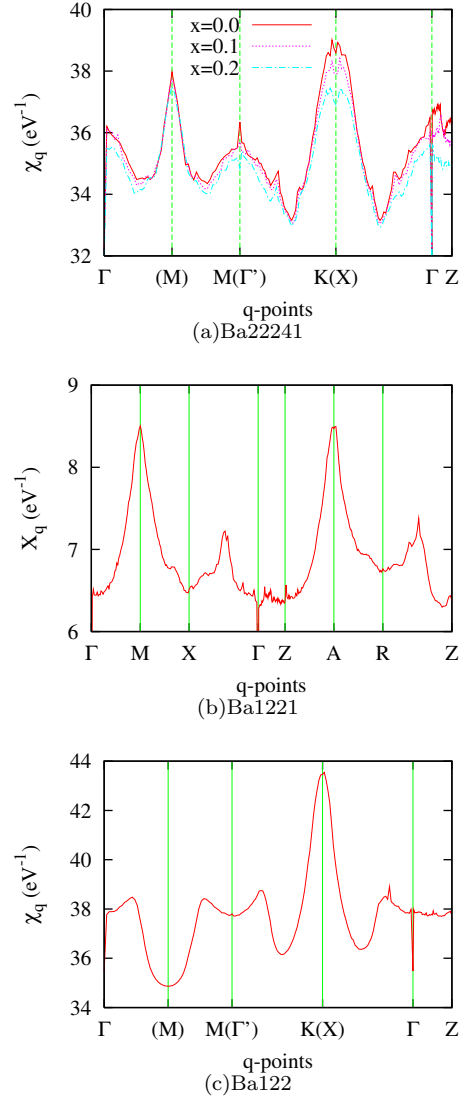


FIG. 4: (Color online) Bare spin susceptibility of (a) $\text{Ba}_2\text{Ti}_2\text{Fe}_2\text{As}_4\text{O}$, (b) $\text{BaTi}_2\text{As}_2\text{O}$, and (c) BaFe_2As_2 . In panel (a), the red solid line, blue dotted line and cyan dash-dotted line are for without doping, $0.1e$ doping and $0.2e$ doping, respectively. For $\text{Ba}_2\text{Ti}_2\text{Fe}_2\text{As}_4\text{O}$ and BaFe_2As_2 , the high symmetry points are labeled according to the Brillouin zone of the body-centered tetragonal primitive cell, the corresponding high symmetry points in the BZ of the tetragonal conventional cell are labeled inside the parenthesis.

the SL-AFM^{Fe} ordering formation is quickly suppressed with electron doping, with a deeper cusp at its center. On the contrary, the $(\pi, 0)$ peak is almost unaffected by the doping. Therefore, the $(\pi, 0)$ instability is in fact more robust than the SL-AFM^{Fe} ordering, and it is most likely to be responsible for the 125-K anomaly.

Interestingly, the $(\pi, 0)$ peak is also present in $\text{BaTi}_2\text{As}_2\text{O}$, whose susceptibility exhibits significant enhancement around M and A , suggesting that the instability is related with the $\text{Ti}_2\text{As}_2\text{O}$ -layers. It is wor-

thy noting here that the $\text{BaTi}_2\text{As}_2\text{O}$ compound has a similar anomaly in the resistivity at $\sim 200\text{K}$ ²². Thus, it is instructive to perform calculations for $\text{BaTi}_2\text{As}_2\text{O}$ compounds. By using PBE0 hybrid functional, we confirm that a checker-board type configuration (Néel-AFM^{Ti}) with $\sim 0.12\mu_B/\text{Ti}$ lowers the total energy by $\sim 13\text{ meV}/\text{Ti}$, which is energetically close to the $\sim 200\text{ K}$ anomaly. As discussed previously, the electronic structure of Ba22241 seems to be well separated into FeAs-related and $\text{Ti}_2\text{As}_2\text{O}$ -related, except for the charge transfer that causes self-doping effect, the Néel-AFM^{Ti} at $\text{Ti}_2\text{As}_2\text{O}$ layers should also be present in Ba22241 . Therefore, the 125K anomaly in Ba22241 is possibly due to a depressed Néel-AFM^{Ti} magnetism at the $\text{Ti}_2\text{As}_2\text{O}$ -layers with small moment. As the formation of magnetic ordering will generally reduce the carrier density, a reduction in the resistivity is expected if the carrier mobility is not enhanced. The scenario is in consistency with the experimental observation.

In conclusion, we have performed electronic structure calculations on the newly-discovered superconductor $\text{Ba}_2\text{Ti}_2\text{Fe}_2\text{As}_4\text{O}$. The presence of intercalated $\text{Ti}_2\text{As}_2\text{O}$ layers induces $0.12e$ charge transfer to FeAs layers, suppressing the formation of the long-range SL-AFM^{Fe} order at the FeAs layer, and causes the 21-K supercon-

ductivity without explicit doping. Bare susceptibility χ_0 exhibits a strong enhancement around M point, which is also present in $\text{BaTi}_2\text{As}_2\text{O}$ compound, suggesting a possible Néel-AFM^{Ti} ordering at the $\text{Ti}_2\text{As}_2\text{O}$ layers in Ba22241 . Therefore, the actual ground state should be a weak AFM in the Ti sublattice and superconducting in the FeAs layers. The coexistence of superconductivity and weak AFM, which develop in the FeAs and $\text{Ti}_2\text{As}_2\text{O}$ layers separately, is due to the almost disentangled electronic structures of the two layers near the Fermi level. How the Ti-AFM affects the superconductivity in FeAs layers, and *vice versa*, seem to be quite interesting, and calls for further studies.

Acknowledgments

This work is supported by NSFC under grant No. 11190023 and 10934005, the National Basic Research Program of China (No. 2010CB923003), as well as NSF of Zhejiang Province No. LR12A04003 and No. Z6110033. All calculations were performed on the High Performance Computing Center of Hangzhou Normal University.

* E-mail address: ghcao@zju.edu.cn

† E-mail address: ccao@hznu.edu.cn

- ¹ Y. Kamihara, T. Watanabe, M. Hirano, and H. Hosono, J. Am. Chem. Soc. **130**, 3296 (2008).
- ² X. H. Chen, T. Wu, G. Wu, R. H. Liu, H. Chen, and D. F. Fang, Nature (London) **453**, 761 (2008).
- ³ D. C. Johnston, Adv. in Phys. **59**, 803 (2010); G. R. Stewart, Rev. Mod. Phys. **83**, 1589 (2011).
- ⁴ C. de la Cruz, Q. Huang, J. W. Lynn, J. Li, W. Ratcliff II, J. L. Zarestky, H. A. Mook, G. F. Chen, J. L. Luo, N. L. Wang, and P. Dai, Nature (London) **453**, 899 (2008).
- ⁵ Q. Huang, Y. Qiu, W. Bao, M. A. Green, J. W. Lynn, Y. C. Gasparovic, T. Wu, G. Wu, and X. H. Chen, Phys. Rev. Lett. **101**, 257003 (2008).
- ⁶ W. Bao, et al., Phys. Rev. Lett. **102**, 247001 (2009).
- ⁷ W. Bao, Q. Huang, G. F. Chen, M. A. Green, D. M. Wang, J. B. He, X. Q. Wang, and Y. Qiu, Chin. Phys. Lett. **28**, 086104 (2011).
- ⁸ M. Rotter, M. Tegel, D. Johrendt, Phys. Rev. Lett. **101** (2008) 107006.
- ⁹ Z. Ren, Q. Tao, S. Jiang, C. M. Feng, C. Wang, J. H. Dai, G. H. Cao, and Z. A. Xu, Phys. Rev. Lett. **102**, 137002 (2009).
- ¹⁰ M. S. Torikachvili, S. L. Budko, N. Ni, and P. C. Canfield, Phys. Rev. Lett. **101**, 057006 (2008).
- ¹¹ H. Ding, P. Richard, K. Nakayama, K. Sugawara, T. Arakane, Y. Sekiba, A. Takayama, S. Souma, T. Sato, T. Takahashi, Z. Wang, X. Dai, Z. Fang, G. F. Chen, J. L. Luo, N. L. Wang, Europhys. Lett. **83**, 47001 (2008).
- ¹² K. Terashima, Y. Sekiba, J. H. Bowen, K. Nakayama, T. Kawahara, T. Sato, P. Richard, Y. M. Xu, L. J. Li, G. H. Cao, Z. A. Xu, H. Ding, and T. Takahashi, Proc. Nat.

- Acad. Sci. USA **106**, 7330 (2009).
- ¹³ D. J. Singh and M.-H. Du, Phys. Rev. Lett. **100**, 237003 (2008).
- ¹⁴ I. I. Mazin, D. J. Singh, M. D. Johannes, M. H. Du, Phys. Rev. Lett. **101**, 057003 (2008).
- ¹⁵ K. Kuroki, S. Onari, R. Arita, H. Usui, Y. Tanaka, H. Kontani, and H. Aoki, Phys. Rev. Lett. **101**, 087004 (2008).
- ¹⁶ S. Raghu, X. -L. Qi, C. -X. Liu, D. J. Scalapino, and S. -C. Zhang, Phys. Rev. B **77** 220503(R) (2008).
- ¹⁷ C. Cao, P. J. Hirschfeld, and H. -P. Cheng, Phys. Rev. B **77**, 220506(R) (2008).
- ¹⁸ F. Ma, W. Ji, J. Hu, Z.-Y. Lu, and T. Xiang, Phys. Rev. Lett. **102**, 177003 (2009).
- ¹⁹ C. Cao and J. Dai, Phys. Rev. Lett. **107**, 056401 (2011).
- ²⁰ Y. L. Sun, H. Jiang, H. F. Zhai, J. K. Bao, W. H. Jiao, Q. Tao, C. Y. Shen, Y. W. Zeng, Z. A. Xu, and G. H. Cao, J. Am. Chem. Soc. DOI: 10.1021/ja304315e.
- ²¹ M. Rotter, M. Tegel, and D. Johrendt, Phys. Rev. B **78**, 020503(R) (2008).
- ²² X. F. Wang, Y. J. Yan, J. J. Ying, J. Q. Li, M. Zhang, N. Xu, X. H. Chen, J. Phys.: Condens. Matter **22**, 075702 (2010).
- ²³ I. Felner, Private communications.
- ²⁴ G. Kresse and J. Hafner, Phys. Rev. B **47**, 558 (1993).
- ²⁵ G. Kresse and D. Joubert, Phys. Rev. B **59**, 1758 (1999).
- ²⁶ P. E. Bloch, Phys. Rev. B **50**, 17953 (1994).
- ²⁷ J. P. Perdew, K. Burke, and M. Ernzerhof, Phys. Rev. Lett. **77**, 3865 (1996).
- ²⁸ I. I. Mazin, M. D. Johannes, L. Boeri, K. Koepernik and D. J. Singh, Phys. Rev. B **78**, 085104 (2008).
- ²⁹ D. J. Singh, Physica C **469**, 418 (2009).
- ³⁰ I. Souza, N. Marzari, and D. Vanderbilt, Phys. Rev. B **65**,

035109 (2001).

- ³¹ A. A. Mostofi, J. R. Yates, Y.-S. Lee, I. Souza, D. Vanderbilt, and N. Marzari, *Comp. Phys. Comm.* **178**, 685 (2008).
- ³² The Ba22241 band structure is fitted using 35 orbitals including Fe-3d, Ti-3d, As-4p and O-2p; BaFe₂As₂ band structure is fitted using 10 Fe-3d orbitals; BaTi₂As₂O band

structure is fitted using 16 orbitals including Ti-3d and As-4p.

- ³³ G. H. Cao et al., *Phys. Rev. B* **82**, 104518 (2010).
- ³⁴ The high symmetry points and all \mathbf{q} -vectors are corresponding to 2-Fe BZ throughout this paper. Therefore $(\pi, 0)$ is the Néel-type AFM, while (π, π) is the SL-AFM.